Multivariable Real-Time Optimal Control of a Cooling and Antisolvent Semibatch Crystallization Process

Milana Trifkovic, Mehdi Sheikhzadeh, and Sohrab Rohani
Dept. of Chemical and Biochemical Engineering, The University of Western Ontario, London, ON N6A 5B9, Canada

DOI 10.1002/aic.11868
Published online July 17, 2009 in Wiley InterScience (www.interscience.wiley.com).

This article presents an experimental study of simultaneous optimization with respect to two variables (cooling rate and flow-rate of antisolvent) in an offline and online (real-time) manner on a semibatch crystallizer. The nucleation and growth kinetic parameters of paracetamol in an isopropanol-water cooling, antisolvent batch crystallizer were estimated by nonlinear regression in terms of the moments of the crystal population density. Moments of crystal population were estimated from the measured chord length distribution, generated by the FBRM®, and the supersaturation was calculated from the measured concentration by attenuated total reflectance-fourier transform infrared spectroscopy. The results of real-time optimization showed a substantial improvement of the end of batch properties (the volume-weighted mean size and yield). For the same objective function, the real-time optimization method resulted in an increase in the volume-weighted mean size by ~100 μm and 15% of theoretical yield compared with the best result obtained in an offline optimization manner. © 2009 American Institute of Chemical Engineers *AIChE J,* 55: 2591–2602, 2009

Keywords: paracetamol-isopropanol-water, antisolvent semibatch crystallization, parameter estimation, nucleation and growth kinetics, offline optimal control, online optimal control, FBRM®, ATR-FTIR

Introduction

Crystallization is a purification and production technique that ensures the product quality in terms of a good size distribution, morphology, and crystalline form to facilitate unit operations placed downstream from the crystallizer. In many applications, control of crystal size distribution is necessary to achieve the desired product properties. External control strategies such as feedback control have been applied to crystallizers to control the concentration, temperature, and crystal size distribution.[1–5]

The evolution of in-line sensors for measuring key process variables such as supersaturation, size, and polymorphic form, opened new directions in the crystallization research. Attenuated Total Reflectance-Fourier Transform Infrared (ATR-FTIR) spectroscopy has been extensively used for the *in situ* measurement of the concentration of the solute in the solution.[6,7]

There has been a growing interest in the use of optimization methodologies to achieve the optimal trajectories for the control of batch crystallization processes. The optimal control of crystallization research was initiated by obtaining the optimal cooling or antisolvent addition trajectories for the crystallizer by offline optimization and then utilizing the feedback control to implement the optimal trajectories.[8–20]

The effectiveness of offline optimal control is reduced due to process-model mismatch, uncertainty in initial conditions,

Correspondence concerning this article should be addressed to S. Rohani at rohani@eng.uwo.ca

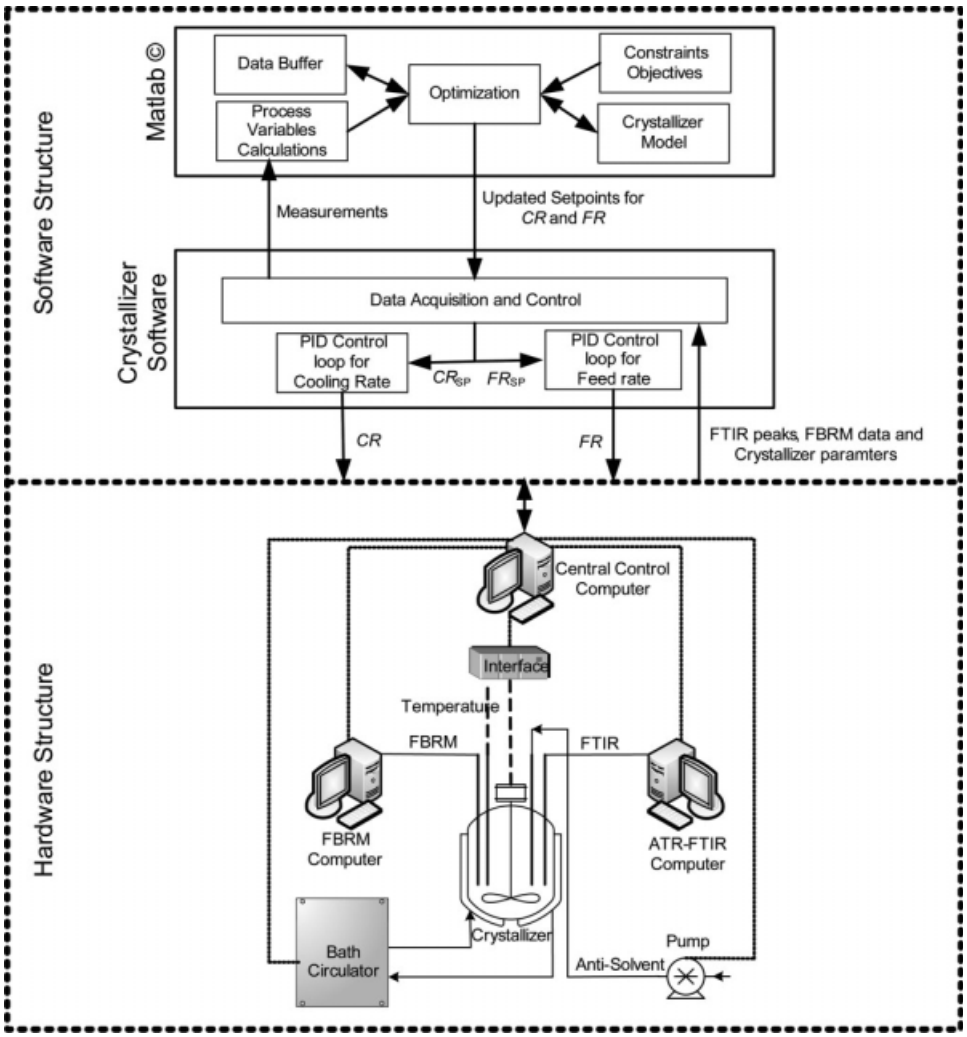

Figure 1. Experimental setup: hardware and software structure.

and batch-to-batch variations. Real-time online optimization addresses some of these issues. The major improvement of this methodology is that the process conditions are continuously updated in each optimization step. This approach is not easy to implement when process is highly nonlinear and unpredictable with large dimensional problems. Corriou and Rohani[21] developed and applied a nonlinear geometric feedback controller by employing an extended Kalman filter for state estimation. Zhang and Rohani[22] continued their work using the extended Kalman filter and developing an online optimal control methodology for the optimal quality control of a seeded batch cooling crystallizer. Sheikhzadeh et al.[23] designed and implemented a real-time single variable optimization procedure on a semibatch crystallization process to obtain the optimal antisolvent feeding rate in a real-time manner.

A significant portion of research and application in the field of process optimization consider a single optimal variable, although most of the real world problems involve more than one variable that have significant effects on the process. On the basis of the properties of the chemicals such as solubility, it is possible to combine several crystallization methodologies (i.e., cooling and antisolvent addition) together to improve the final batch properties and product yield. In batch crystallization, combining these two methodologies has a major effect on the yield of process, since this synergistic action results in providing extra driving force for the crystallization process. However, this synergistic action also has an effect on the rate of nucleation and growth of particles and could result in poor end-of-batch properties if the process is not controlled well. It is desirable to optimize the end-of-batch properties and simultaneously maximize the product yield by combining different crystallization methodologies. This task can be achieved by using either feedback controllers to control some process variables such as supersaturation or by applying the optimal control strategies. Recently, a neuro-fuzzy logic feedback controller was utilized to control the supersaturation and the number of particles in a given chord length range, in combination of antisolvent and cooling crystallization.[24]

This work deals with an experimental study of model-based offline and online (real-time) multivariable optimal control of a semibatch unseeded crystallization process. Two crystallization strategies, cooling and antisolvent, were used

Table 1. Experimental Conditions

Variable	Name	Value	Units
k_v	Shape factor	1.5	–
m_{IPA+H_2O}	Initial mass of solvent mixture	300	g
ρ_c	Crystal density	1293	kg/m^3
C_0	Initial concentration	≥ 0.25	$g_{solute}/g_{solvent(IPA+H_2O)}$
C	Concentration	0.0035*P(946)/P(1307) + 0.4411*P(1380)/P(1307) + 0.1046*P(1513)/P(1307) − 0.2149 *P(1243)/P(1307) + 0.0018*T − 0.4051	$g_{solute}/g_{solvent(IPA+H_2O)}$
C^*	Solubility	$0.208 - 0.254*m_w + 0.009$ *T + 0.039 $*m_w + 6.5403 \times 10^{-5}$*$T^2 - 0.0122$ $*m_w$*T	$g_{solute}/g_{solvent(IPA+H_2O)}$
T_{start}	Temperature	40	°C
T_{end}	Temperature	10	°C

P(*) is the FTIR peak at the * wave number.

simultaneously, and the optimization procedure was applied to obtain the best optimal trajectories for cooling and antisolvent rates in offline and online manners. Before the optimization step, crystallization kinetics were estimated from the experimental data to solve the crystallization model. The optimal control algorithm has the ability of constraint-handling in a feedback manner to adapt the optimal strategy to the real process conditions. Several objective functions and their combinations were used. Their effect on the final product batch properties and yield was studied as well.

Experimental Methods

Figure 1 shows the hardware and software structure of the experimental setup used in this study. Experiments were performed in a 1-L bench scale, antisolvent, batch crystallizer system. The in situ FBRM® probe (Mettler Toledo, Redmond, WA) was used for acquiring the chord length distribution (CLD) data. Twelve consecutive samples taken every 5 s were averaged to render the CLD data. An in situ ATR-FTIR (Hamilton Sundstrand, CA and DMD-270 diamond ATR immersion probe) was used to collect online infrared spectra. The FTIR spectra were related to the solute concentration in the solution using the calibration curve developed by Sheikhzadeh et al.[5] The crystal size distribution (CSD) of the final product was measured by Malvern 2000 SCIRRCCO (Malvern Instruments Ltd., UK). A metering pump (Gala 1602) was used for pumping water, which was used as an antisolvent in the crystallization process. An electronic balance (Oxford, B41002) was used for recording the amount of the antisolvent added to the solution. A supervisory controller was used to control the crystallizer temperature and antisolvent feeding rate. More detailed description of the experimental set-up is given in Trifkovic et al.[20] All experiments discussed in this article were unseeded crystallization runs. Before running the experiments, the ATR-FTIR chamber was purged for 12 hr using filtered air (CO_2 and H_2O free) to stabilize the background. The FTIR chamber was filled with liquid nitrogen as inert gas. The solution containing 120 g of IPA and 180 g of water saturated with 74.3 g of paracetamol at 40°C was added in the jacketed vessel. Stirrer speed was maintained at 200 rpm throughout the experiments, and it provided good mixing while avoiding excessive splashing. The clear solution was initially kept above the saturation temperature at 44°C. The temperature was then lowered to 40°C to start the experiments. The temperature was held constant at 40°C for 15 min (that corresponded to $t = 0$) before the addition of a total of 300 g of the antisolvent (water) and cooling of crystallizer content from 40 to 10°C in all experiments. At the onset of each experiment, the FBRM® counts showed a nil value. The experimental conditions are shown in Table 1. At the end of each experiment the slurry was withdrawn, filtered through a 1 μm filter. The crystals were dried, and their size distribution was measured by the Malvern Mastersizer.

Nucleation and growth parameters estimation methodology

To estimate the crystallization kinetic parameters, growth and nucleation rates had to be measured or calculated. In this study, FBRM® and ATR-FTIR spectroscopy were utilized to measure CLD and solute concentration, respectively. The growth and nucleation rates were approximated in terms of the moments obtained from the measured CLD directly, without converting the CLD measurements to the particle size distribution (PSD). The CLD data can be converted to PSD under certain assumptions such as known particle shape and that the particles backscatter the light at all angles. However, for irregular particles such conversion is not straightforward. An alternative approach is to calculate the low-order moments from the CLD directly without converting the CLD data to PSD. The justification for this is that the mapping between the PSD and CLD is static for low-order moments, and thus theoretically they should follow the same trend. The moments of CLD were calculated as follows:

$$\mu_k(t) \equiv \int_0^\infty r^k n(r,t)dr \approx \sum_{i=1}^{\text{FBRM final channel}} r_{\text{ave},i}^k N_i(r_{\text{ave},i}, j) \quad (1)$$

where r_i and N_i are the chord length and number of particles in channel i, respectively. j is the discrete time counter. $r_{ave,i}$ is the average of chord length between two consecutive channels (i and $i+1$).

The 0th CLD moment was used to approximate the nucleation, and the ratio of first to zeroth CLD moment was used for the growth rate approximation.

$$G_{\text{exp},j} = \left[\frac{d\left(\frac{\mu_1}{\mu_0}\right)}{dt}\right]_j = \left[\frac{d(\overline{L}_{1,0})}{dt}\right]_j \approx \left[\frac{\Delta\overline{L}_{1,0}}{\Delta t}\right]_j \tag{2}$$

where L is the mean crystal size, μ_1 and μ_0 are first and 0th CLD-based moments of the population density. The total number of crystals in the whole FBRM® size range (1–1000 μm) was used to approximate the nucleation rate.

$$B_{\text{exp},j} = \frac{1}{M_j}\cdot\frac{dN}{dt} \approx \frac{1}{M_{\text{initial}} + M_{\text{antisolvent},j}}\cdot\frac{\Delta N_j}{\Delta t_j} \tag{3}$$

where B_j, M_j, and N_j are the nucleation rate, total mass of solvent, and total number of crystals in the jth sampling time interval, respectively. The approximation of nucleation and growth rates is improved if one includes the ratio of the volume traced by the laser beam of the FBRM® to the total crystallizer volume. The approximation is justified since it is based on the relative chord length counts between two consecutive sampling intervals, and not on the absolute counts at each sampling interval. The detailed approximation procedure of growth and nucleation rates is given by Trifkovic et al.[20]

Growth and nucleation rates are functions of temperature and mass of antisolvent, as well as the main driving force for crystallization process, supersaturation (ΔC).

$$G_{\text{pred},j} = k_g \Delta C_j^g \tag{4}$$

$$k_g = k_{g0}\exp\left(\frac{E_g}{RT_j}\right) \tag{5}$$

$$g = g_1 m_{w,k} + g_2 \tag{6}$$

$$B_{\text{pred},j} = k_b \Delta C_j^b \tag{7}$$

$$k_b = k_{b0}\exp\left(\frac{E_b}{RT_j}\right) \tag{8}$$

$$b = b_I m_{w,k} + b_2 \tag{9}$$

where the subscript j refers to the sampling time. As seen from Eqs 4–9, there are four parameters to be estimated for the growth (G_{pred}) and nucleation (B_{pred}) rates. Growth and nucleation constants k_g and k_b are functions of temperature, whereas b and g are functions of antisolvent mass percent (m_w). The kinetic parameters were estimated based on the experimental data acquired from five open loop experiments, which were performed by applying different cooling and antisolvent rate trajectories. Three linear profiles (with a zero, negative, and positive slope), and two nonlinear, parabolic in shape, cooling rate and antisolvent flow-rate profiles were applied. The batch time (120 min), temperature range (40–10°C), and the amount of antisolvent added to the crystallizer (300 g) were fixed for the experiments.

A nonlinear least squares optimization technique was used to estimate kinetic parameters for growth and nucleation rates as follows:

$$J_G = \min_{(k_g,E_{ag},g_1,g_2)} \frac{1}{2}\sum_{j=1}^{t_{\text{final}}} \times \left(G_{\text{pred}}((k_g, E_{ag}, g_1, g_2), (T, m_w, \Delta C)) - G_{\text{exp}}\right)^2 \tag{10}$$

$$J_B = \min_{(k_b,E_{ab},b_1,b_2)} \frac{1}{2}\sum_{j=1}^{t_{\text{final}}} \left(B_{\text{pred}}((k_b, E_{ab}, b_1, b_2), (T, m_w, \Delta C)) - B_{\text{exp}}\right)^2 \tag{11}$$

The parameters were estimated by applying the optimization technique to the entire data obtained from the beginning to the end of the batch (t_{final}).

Batch crystallization model

Crystallization dynamics can be described by population balance equation, energy balance, and mass balances on solute and solvent.

The population balance for a batch crystallizer in which crystals are born at size zero, particle growth is size independent, crystal agglomeration and breakage are neglected, and crystal shape is uniform can be represented by Randolph and Larson.[25]

$$\frac{\partial n(r,t)}{\partial t} + G(t)\frac{\partial n(r,t)}{\partial r} = 0 \tag{12}$$

The solute balance for a batch crystallizer is

$$\frac{dC}{dt} = -3\rho k_v G(t)\mu_2(t) \tag{13}$$

where, ρ is the solid density, k_v is the shape factor, and μ_2 is the second moment of the PSD. The solid density and shape factor are both assumed to be constant, and their values are given in Table 1. The detailed procedure for calculation of the second moment can be found in Trifkovic et al.[20]

The boundary and initial conditions are given by:

$$n(r,0) = n_0(r) \tag{14}$$

$$n(0,t) = \frac{B(t)}{G(t)} \tag{15}$$

$$C(0) = C_0 \tag{16}$$

where C_0 is the initial concentration of the solute in the solvent, and n_0 is the population density of nuclei at size zero. Assuming uniform crystal shape, the PSD and the CLD were assumed to have a parabolic shape given by Hu et al.[17]:

$$n(r,0) = \begin{cases} 0.0032(r_{\text{final}} - r)(r - r_{\text{initial}}) & r_{\text{initial}} \le r \le r_{\text{final}} \\ 0 & \text{elsewhere} \end{cases} \tag{17}$$

Since we are dealing with an unseeded crystallization process, the initial condition for CLD of seeds was zero. At the onset of nucleation, the CLD of nucleated crystals (estimated

Table 2. Objectives, Constraints and Goals for Optimization

	Variable	Description
Objectives		
J_1	$\frac{B}{G}$	Minimizing nucleation and maximizing growth
J_2	$\frac{\mu_3}{\mu_2}$	Minimizing ratio of third to second moment
J_3	$\sqrt{\frac{\mu_3\mu_5}{(\mu_4)^2}-1}$	Minimizing a coefficient of variation
Constrains		
c_1	$t_{\text{final}} = t_{\max} = 120$ min	Final batch time is fixed
c_2	$T(\text{end}) = 10$	Final crystallizer temperature is fixed
c_3	$m_w(\text{end}) = 0.8$	Final antisolvent mass percentage is fixed
c_4	$\frac{dFR}{dt} \leq 0.5$	Constraints for Flow-rate gradient
c_5	$0.5 < FR < 9$	Flow-rate must be within the predetermined limits
c_6	$0.1 < CR < 1$	Cooling rate must be within the predetermined limits
c_7	$\frac{dCR}{dt} \leq 0.25$	Constraints for cooling rate
Goals		
λ_1	2×10^6	Initial goal for J_1
λ_2	1×10^2	Initial goal for J_2
λ_3	5×10^{-2}	Initial goal for J_3

based on FBRM® data), was treated as seeds for the consecutive optimization process. The procedure was repeated until the end of the experiment.

Objectives and constraints of the optimization problem

In crystallization, a principal determining factor for the product quality is the final PSD. Hence, the objectives chosen in the optimization problem were closely related to factors that directly affected the final PSD, such as minimization of nucleation (J_1 and J_2) during the crystallization process and coefficient of variation (J_3).

Given that there are two input variables in this system, cooling water rate (CR) and antisolvent flow rate (FR), the single objective optimal control problems can be represented as follows:

$$\begin{aligned} &\min_{\text{FR}} J_1 \quad \text{LB}_{\text{FR}} \leq \text{FR} \leq \text{UB}_{\text{FR}} \quad (l = 1,2,3) \\ &\min_{\text{CR}} J_1 \quad \text{LB}_{\text{CR}} \leq \text{CR} \leq \text{UB}_{\text{CR}} \quad (l = 1,2,3) \end{aligned} \tag{18}$$

where l is the scenario number. The crystallization process was also subjected to the set of equality (c_{eq}) and inequality (c_{neq}) constraints which can be represented as:

$$c_{\text{eq}}([T, m_w, t]_{\text{final}}) = 0 \tag{19}$$

$$c_{\text{neq}}\left(\frac{d\text{FR}}{dt}, \frac{d\text{CR}}{dt}\right) \leq 0 \tag{20}$$

Optimization functions and constraints are listed in Table 2. A number of goals associated with different objective functions are also listed in Table 2.

Since the crystallization model is highly nonlinear, and the process is subjected to the set of algebraic equality and nonequality constraints mentioned above, the optimization problem presented here falls in the category of a constrained nonlinear programming problem (NLP).

Optimal control strategy

As mentioned before, optimal control strategy was performed in an offline and online manner. Offline optimization refers to first finding the optimal trajectories for cooling rate and antisolvent flow-rate in the simulation environment, and then implementing those trajectories to the process. Online optimal control refers to finding these optimal trajectories successively at each control interval until the end of the batch and implementing the first segment of the optimal path in one control interval immediately after the computation. This procedure is repeated in the next control interval with the updated information received from the crystallizer. Two PID controllers (one on the cooling water flow rate and the second one on the flow rate of antisolvent, to the crystallizer) were utilized to implement these optimal trajectories as a series of consecutive set-points until the end of batch.

In an online optimization problem in general, three distinct time intervals are involved:

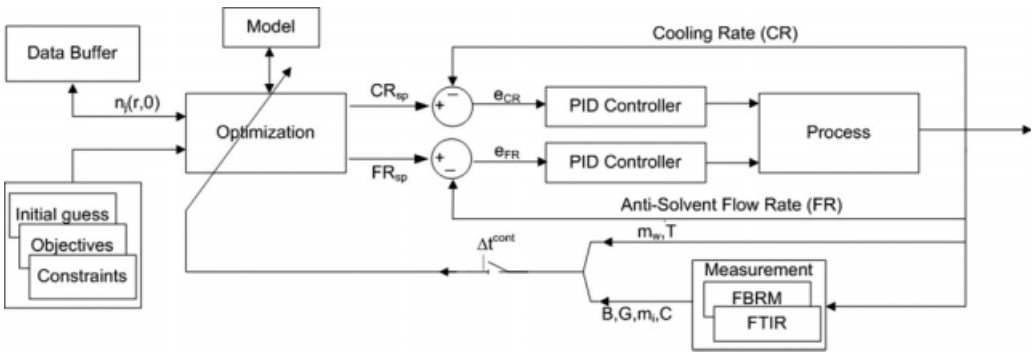

Figure 2. Optimal control strategy.

Table 3. Estimated Kinetic Parameters

Rate	Kinetic Parameters	Value ($\alpha = 0.05$)
Growth	k_{g0}	$2.34 \times 10^{-6} \pm 2.61 \times 10^{-7}$
	E_g	$1.01 \times 10^{2} \pm 4.50$
	g_1	$9.75 \times 10^{-2} \pm 12.6 \times 10^{-3}$
	g_2	1.01 ± 0.08
Nucleation	k_{b0}	46.93 ± 6.75
	E_b	$7.28 \times 10^{2} \pm 55.65$
	b_1	-5.26 ± -0.68
	b_2	4.53 ± 0.27

• Δt_{samp}—the sampling time interval (set to 1 minute), which represents the time interval of measurement (designated by j).

• Δt_{opt}—the optimization time interval (set to 1 minute), which represents number of optimization segments in the calculated optimal profiles.

• Δt_{cont}—the control interval (also set to 1 minute and designated by k), in which the first value of the new calculated optimal profile is implemented to the system.

Figure 2 depicts a feedback control scheme that was used to implement the online optimal trajectory found by the optimization algorithm. In each sampling interval, Δt_{samp}, data acquired by FTIR, FBRM® (see Measurement block in Figure 2), along with the measured temperature (T), and mass of solvent data (m_w), were used to estimate the moments of the CLD, growth, nucleation, and solute concentration. Equations 4 and 7 were used to approximate the nucleation and growth rates for the model simulation until the end of batch.

Values of these variables were fed to the Optimization block (Figure 2) in each Δt_{cont}. Model based optimization was performed using auxiliary optimization requirements (Objectives, Initial guess, Constraints block in Figure 2). Data Buffer block provided the initial seed size distribution

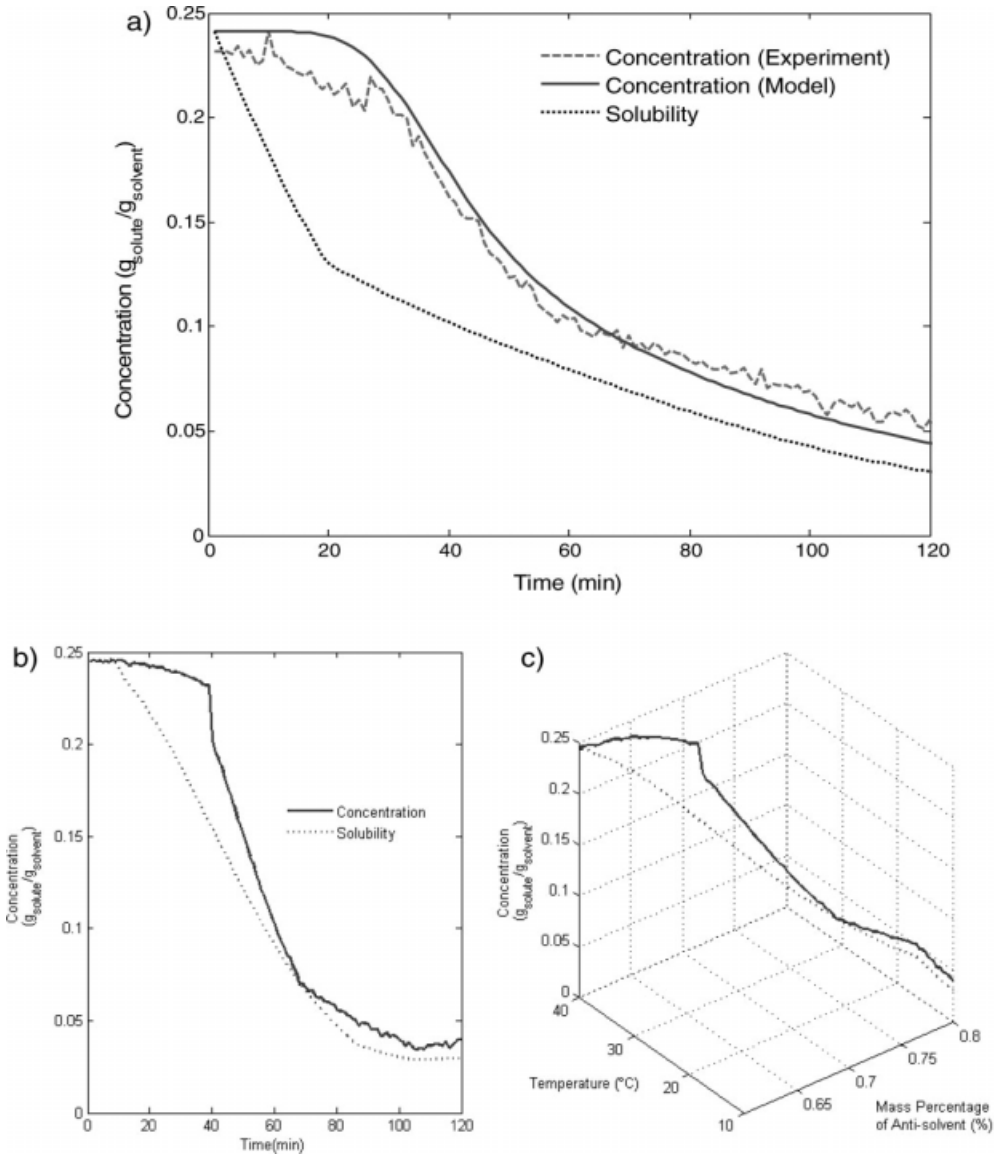

Figure 3. Concentration profile for S1.

a) Offline optimal control as a function of time b) online optimal control as a function of time, c) online optimal control as a function of temperature and mass-percentage of antisolvent.

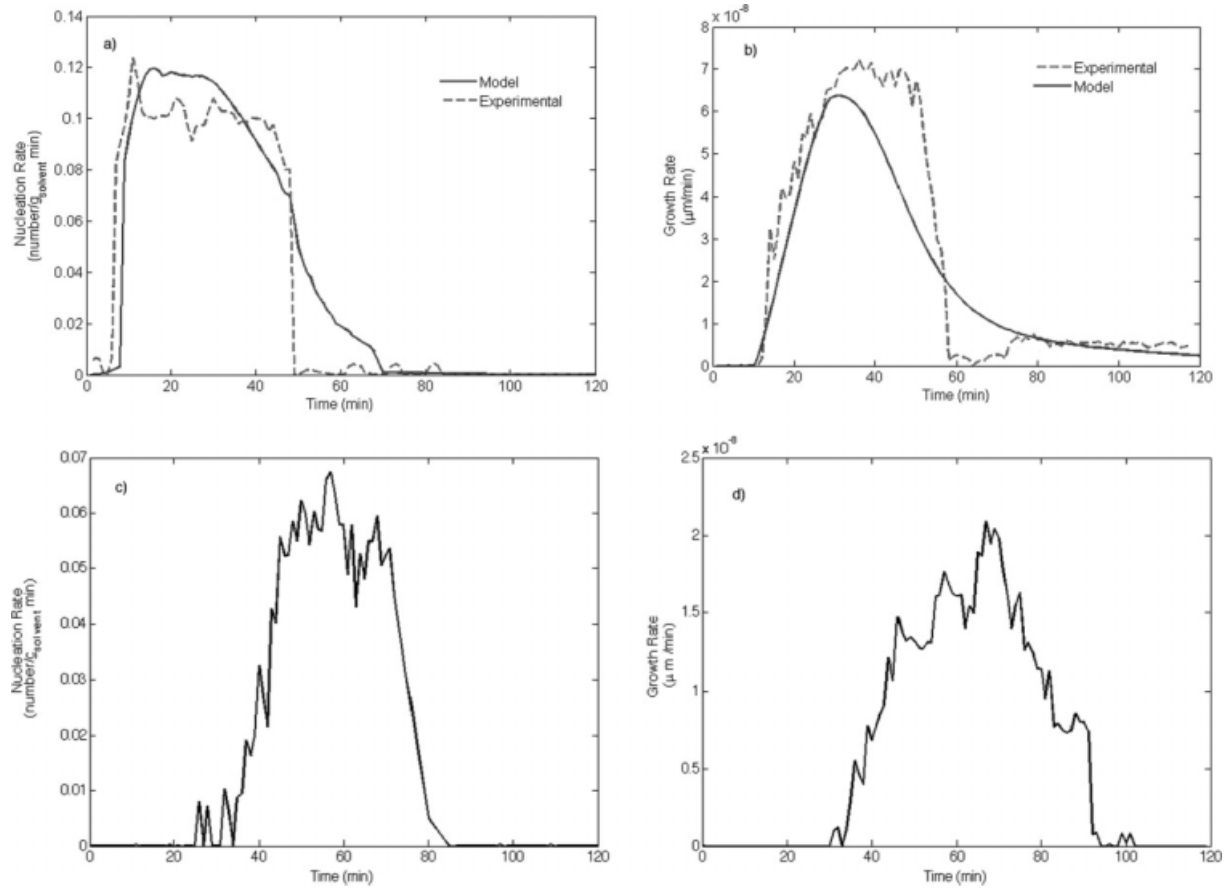

Figure 4. Offline optimal control for S1: a) Nucleation rate, b) Growth rate. Online optimal control for S1: c) Nucleation rate, d) Growth rate.

obtained from the previous Δt_{cont}. The outputs of the Optimization block at each control time interval, Δt_{cont}, were two optimal trajectories (CR and FR). The initial estimates for both trajectories were assumed to be linear with values of 3 g/min for FR, and 0.25°C/min for CR, respectively. They were calculated from the current time, j, until the end of batch (t_{final}). However, only the first segments of the two calculated trajectories ($k = 1$) were implemented on the system as updated setpoints (CR_{sp} and FR_{sp}) for the two local PID loops (Figure 2). The current temperature and mass of antisolvent added to the crystallizer was then calculated based on the updated setpoints.

All the calculation regarding the optimization and modeling were performed using MATLAB computational software. The MATLAB optimization function, fmincon, was used to solve the single objective NLP problem for two optimal variables and the solution methodology used was based on the sequential quadratic programming (SQP) method.

For multiobjective optimization problems, MATLAB optimization function fgoalattain was found to be the most appropriate. The selection was made mostly on the computation time restriction, which can become a limiting factor in case of the online multiobjective optimization. The optimal trajectory had to be computed and implemented in 1 minute, and fgoalattain is shown to be acceptable according to both the obtaining desired optimal trajectories, and meeting the computation time restriction. It is based on SQP method and requires the construction of a vector of objective functions and vectors of goals associated with them. The weights for each objective function should be assigned, and in this case they were all set to be equal to one, so that each objective function was given the same significance in the optimization process. The applied goal attainment multiobjective optimization was as follows:

$$\begin{cases} \underset{\text{FR,CR}}{\text{minimize}}\ \gamma \\ \text{with}\,(J_1 - \gamma) \le \lambda_1 \\ \quad\vdots \\ \text{subject to}\, c_1 \text{to}\, c_7 \end{cases} \tag{21}$$

which λ is the optimization goal and γ is the factor which needs to be minimized. This is also called an unscaled goal attainment problem. By minimizing the γ, the objective functions converge to the goal (λ). The values of goals are given in Table 2, and their values were determined based on the knowledge gained from the set of open loop experiments.

Results and Discussion

Optimal profiles obtained from the offline optimal control were implemented during the entire batch and served for

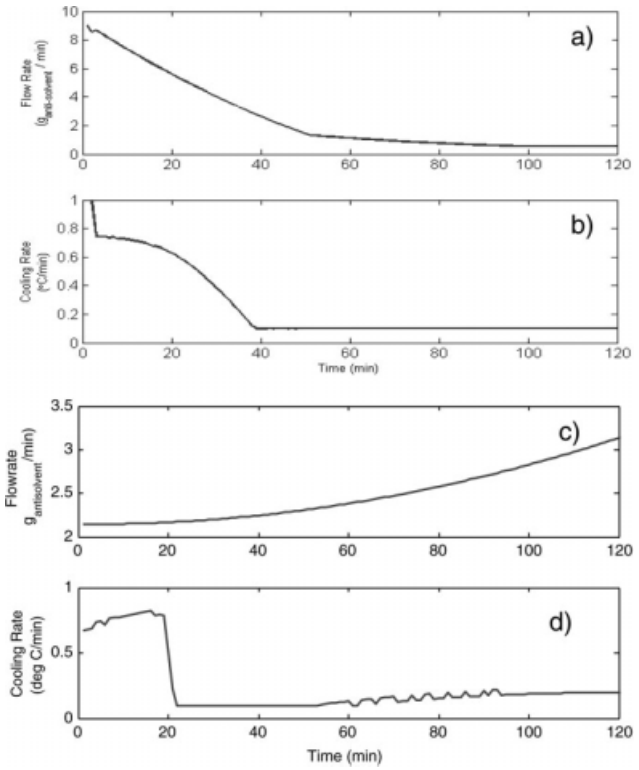

Figure 5. Optimal profiles for S1.

Offline optimal control: a) Antisolvent flow-rate (FR), b) Cooling rate (CR). Online optimal control: c) Antisolvent flow-rate (FR), d) Cooling rate.

comparison with the real-time optimal control. On the basis of the procedure described in the third section, kinetic parameters were estimated, and their values along with their 95% confidence intervals are presented in Table 3. These parameters were used to solve and validate the crystallization model. After model validation was performed (using open loop experiments), the offline and online optimal control studies were conducted.

Comparison between offline and online optimal control strategies

In this section, comparison between the offline and online optimal control strategy for two different scenarios is discussed. As stated in the the sixth section, the main difference between the two strategies was the method of implementation of the optimal profiles for FR and CR. Various scenarios mentioned in Table 2 were used, but Scenario 1 and 2 (both multiobjective cases) resulted in better optimization performance for offline optimal control strategies. Thus, they were chosen to also be further studied in the real-time optimization and for comparison of two different strategies. Five repetitions of experiments for each Scenario were performed as well, and the results were within 10% difference in terms of the final batch properties, such as the final PSD and yield.

Scenario 1. Scenario 1 was defined in terms of the nucleation and growth rate as well as the ratio of the third to second moment of crystallization (J_1 and J_2). The optimization problem formulation was

$$S_1 = \begin{cases} \underset{\text{FR,CR}}{\text{minimize}}\ \gamma \\ \text{with}\ (J_1 - \gamma) \le \lambda_1 \\ \qquad (J_2 - \gamma) \le \lambda_2 \\ \text{subject to}\ c_1\ \text{to}\ c_7 \end{cases} \tag{22}$$

The goal values (λ) are given in Table 2. The minimization of such objective functions results in suppressing the nucleation and enhancing the growth rate. A typical concentration profile obtained by applying this scenario in an offline and online manner is shown in Figure 3. As seen from Figure 3a, the modeled solute concentration profile was in close agreement with the experimental solute concentration data, which also served as an additional evidence for the validation of the crystallization model and all the assumptions employed. It can be seen from the figure that the supersaturation increased at the beginning of the experiment until the onset of the primary nucleation, and thereon was used for the growth of newly nucleated particles. Note that the experiments were unseeded crystallization, and, thus, the supersaturation was not used until the primary nucleation took place. The concentration trend as a function of time and manipulated variables for S_1 applied in an online manner is shown in Figures 3b, c. The first obvious difference in the concentration trend for the case of online optimal control is that the supersaturation was used more effectively until the end of the experiment.

The modeled and experimental data for growth and nucleation obtained by offline optimal control strategy (Figures 4a, b)

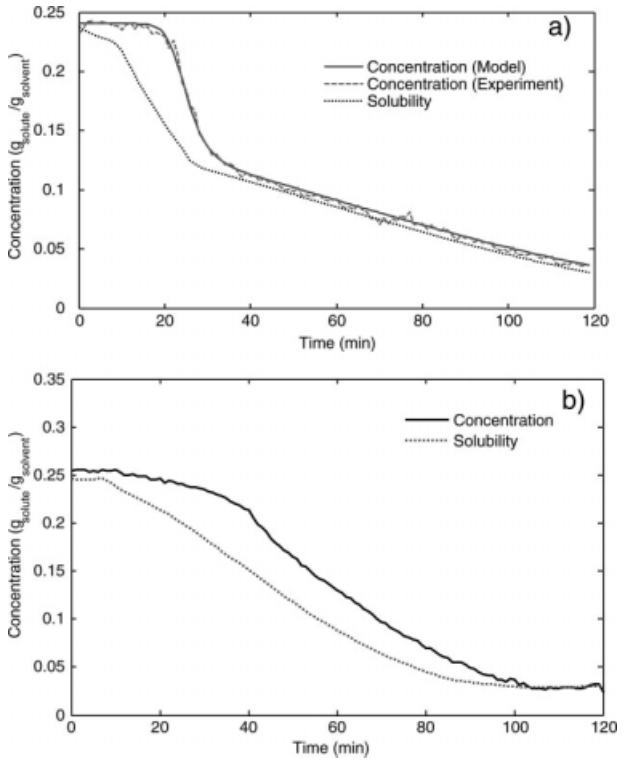

Figure 6. a) Concentration profile for S2—offline optimal control, b) Concentration profile for S2—online optimal control.

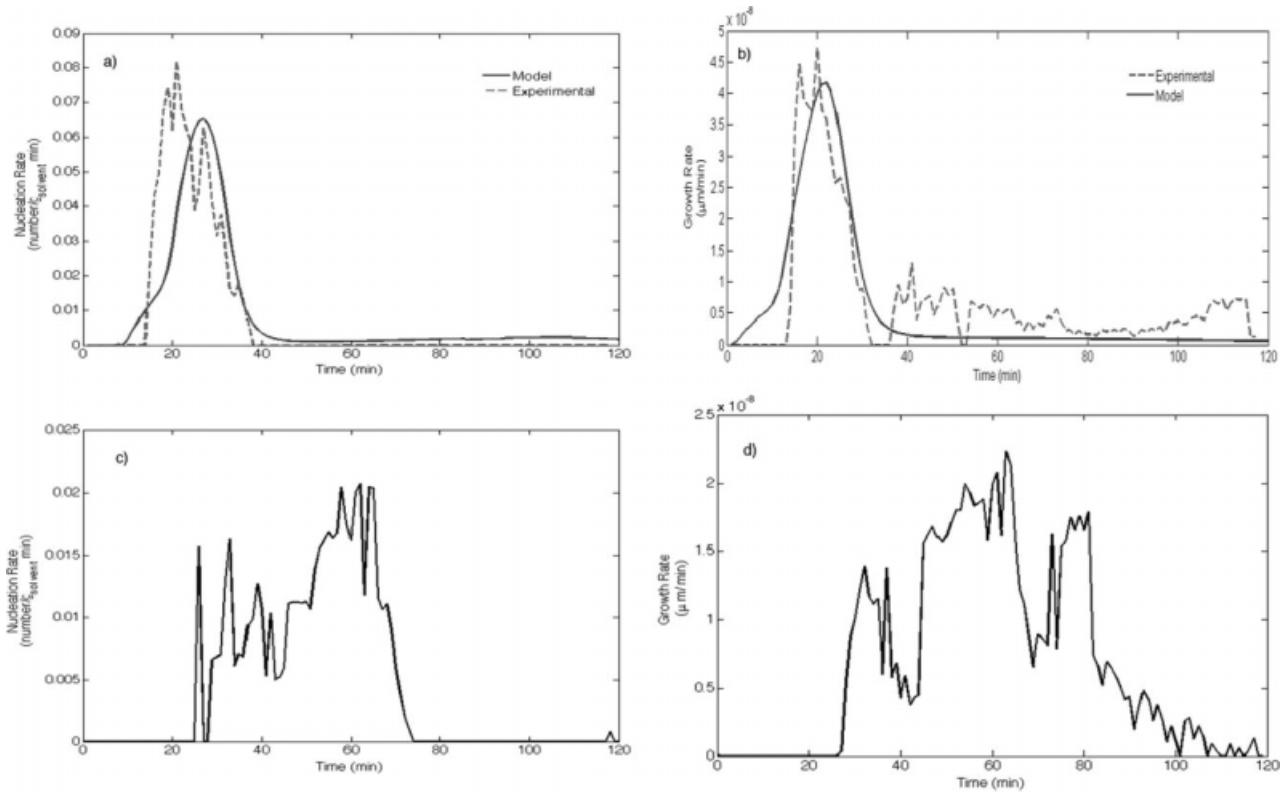

Figure 7. Offline optimal control for S2: a) Nucleation rate, b) Growth rate. Online optimal control for S2: c) Nucleation rate, d) Growth rate.

are in close agreement with respect to the magnitude, and the time interval for each of the events. The difference in the shape of the experimental and predicted growth and nucleation rates suggests that the model cannot predict all of the process events and there is a need for an online optimal control. The magnitude of nucleation rate for an online optimal control strategy (Figure 4c) decreased in comparison to the same experiment by implementing the optimal profiles obtained in an offline manner. Growth rate trend for online optimal strategy, shown in Figure 4d also confirms the more effective use of supersaturation since the growth of particles occurred for a longer period of time in comparison to the experiment performed in an offline manner.

The optimal profiles for cooling rate and antisolvent flow-rate for offline strategy (Figures 5a, b) showed the highest rates of both manipulated variables at the beginning of the experiment and then a slow decrease after the onset of nucleation. However, the same results for online strategy (Figures 5c, d) show more sensitivity to the process conditions, which is expected considering that they were calculated in an online manner. Cooling profiles have similar trend, but the antisolvent profile obtained by the online optimal strategy is exponentially increasing, whereas for offline strategy the resulting profile has a decreasing trend.

Scenario 2. Scenario 2 contains the minimization of the coefficient of variation (J_3) in addition to the previously described two objectives. The optimization problem formulation is

$$S_2 = \begin{cases} \underset{\text{FR,CR}}{\text{minimize}} \ \gamma \\ \text{with} \ (J_1 - \gamma) \leq \lambda_1 \\ \qquad (J_2 - \gamma) \leq \lambda_2 \\ \qquad (J_3 - \gamma) \leq \lambda_3 \\ \text{subject to} \ c_1 \ \text{to} \ c_7 \end{cases} \tag{23}$$

The solute concentration trends for offline and online optimal control strategies are shown in Figure 6. The results obtained by offline optimal control strategy show that at the end of the experiment the supersaturation was only slightly above the solubility point. This was desired since supersaturation was efficiently used for the growth of particles. The concentration trend for online optimal control strategy shows that the supersaturation was created and used efficiently until the end of the experiment.

The synergistic effect of these three objective functions was obvious in the results for nucleation and growth rates. It can be seen that the nucleation rate magnitude was lowered drastically (Figure 7a) and also the duration of the primary nucleation event was decreased. The growth rate was also enhanced (Figure 7b). The growth and nucleation rate trends confirm that the supersaturation was used significantly after the nucleation reached its maximum peak. The nucleation and growth trends for online optimal control strategy are shown in Figures 7c, d. The first observation that can be made from these graphs is that the magnitude of nucleation is drastically decreased and that growth time is prolonged in

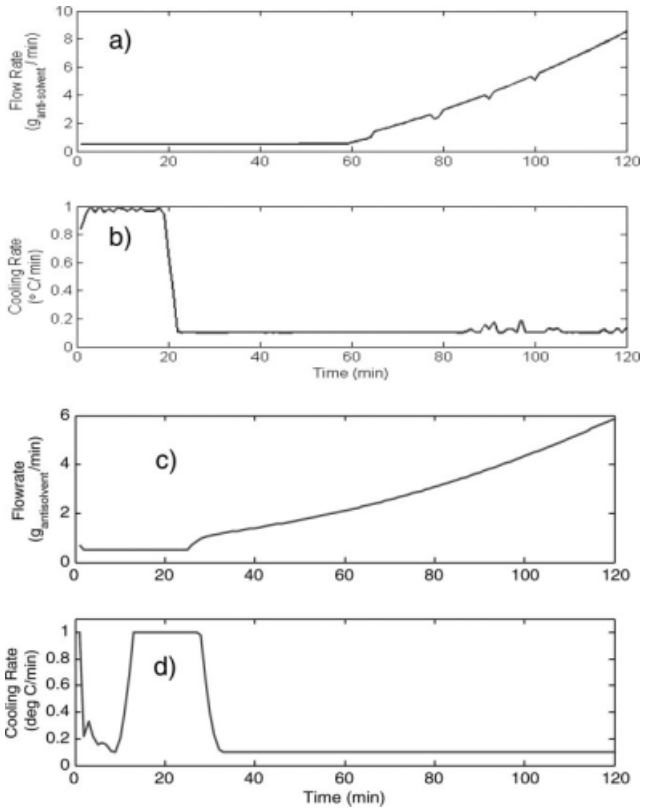

Figure 8. Optimal profiles for S2.

Offline optimal control: a) Antisolvent flow-rate (FR), b) Cooling rate (CR). Online optimal control: c) Antisolvent flow-rate (FR), d) Cooling rate (CR).

comparison to the results obtained by offline optimal control strategy.

Optimal profiles depict the synchronized action of two optimal control variables for keeping the supersaturation level at the optimal point (Figure 8). As seen from Figure 8b, at the beginning of the experiment, the cooling rate was at the high level (to produce sufficient amount of supersaturation for the primary nucleation), whereas the antisolvent flow-rate was at the low level. As the flow-rate increased, the cooling-rate was kept at the low level, so that the concentration stayed within the detectable zone. This can also be proved by the fact that after the primary nucleation, the occurrence of nucleation events was kept at minimum. Optimal profiles for online optimal control strategy are illustrated in Figures 8c, d. Although the trend of these curves are similar to the ones obtained in an offline manner for the same scenario, the sensitivity and speed of response to the process conditions (i.e., occurrence of nucleation) is more obvious, and as such resulted in minimizing the nucleation rate significantly. The antisolvent flow-rate shows that the rate of the antisolvent was very high toward the end of the experiment, which produced sufficient amount of supersaturation until the end of the experiment, and thus resulted in keeping the growth of particles active until the end of the experiment.

Scenario 3. The last scenario investigated was a single objective case (S_3) for a fair comparison with the multiobjective cases performed in offline manner. The single objective optimization formulation for this scenario is

$$S_3 = \begin{cases} \underset{\text{FR,CR}}{\text{minimize}}\, J_1 = \frac{B}{G} \\ \text{subject to } c_1 \text{ to } c_7 \end{cases} \tag{24}$$

The concentration trend shown in Figure 9 illustrates that the supersaturation was not used as effectively as in the two multiobjective optimization cases performed in an online manner. However, the magnitude of nucleation rate (Figure 10a) was still in the range of the best multiobjective case performed in an offline manner, and the growth of particles (Figure 10b) took place for a longer period of time. Optimal profiles shown in Figure 11 had an opposite trend to the multiobjective cases, which confirms the synergistic effect of several objectives. In this case, only the minimization of nucleation was considered as the objective, and the outcome of the control methodology was significantly different in comparison with the multiobjective cases performed by an online optimal control approach.

Final product quality comparison between online and offline strategies

To adequately evaluate the performance of each control strategy, comparison of results in terms of process kinetics (growth and nucleation rates) as well as the final batch properties (yield and final CSD) was performed. The integration of the growth and nucleation rates over the entire batch time, was executed for the purpose of comparing the results in a quantitative manner:

$$B_{\text{accumulated}} = \sum_{j=1}^{t_{\text{final}}} B_j \tag{25}$$

$$G_{\text{accumulated}} = \sum_{j=1}^{t_{\text{final}}} G_j \tag{26}$$

It can be noted that the volume-weighted average of the final CSD is significantly larger (>90 μm) for the same objective functions experiments performed in an online

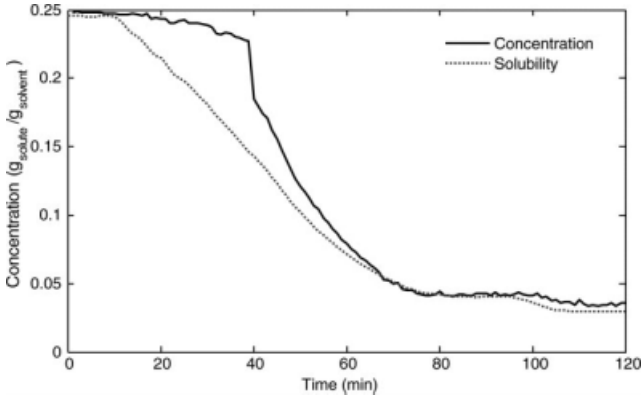

Figure 9. Concentration profile for S3—online optimal control.

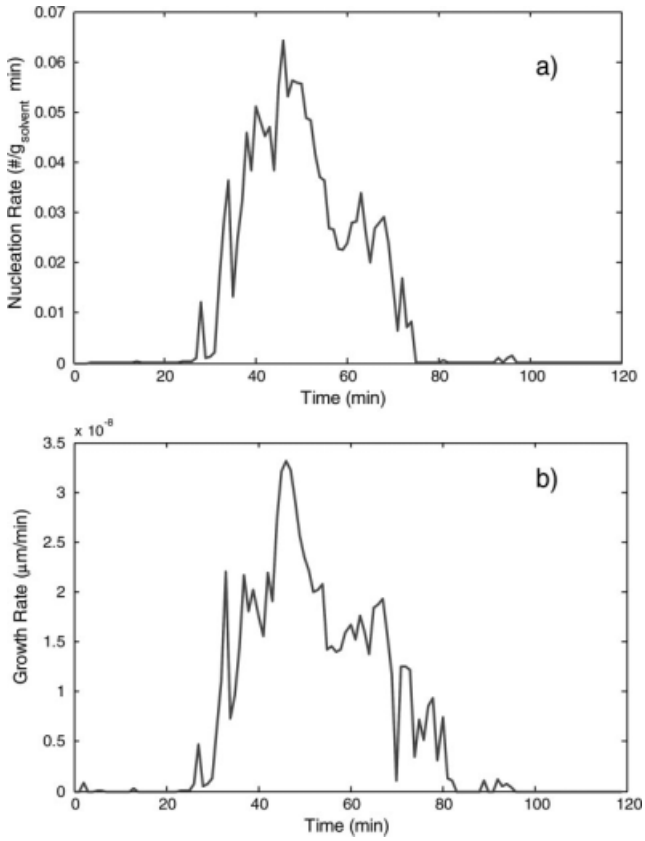

Figure 10. Nucleation (a) and Growth rate (b) for S3—online optimal control.

manner (Table 4). This can be attributed to the fact that the nucleation rate was higher for experiments performed in an offline manner. Although the growth rate for these experiments was considerably high, the excessive number of very fine particles at the onset of the primary nucleation caused the mean particle size to be significantly lower at the end of the experiment. Yields of experiments performed in the online approach were also higher by approximately 15% (for

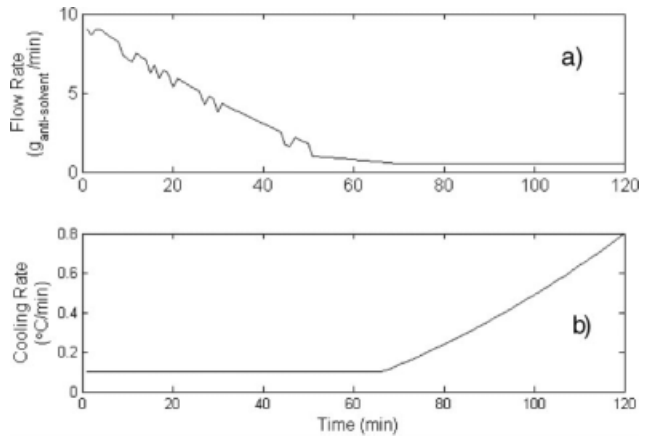

Figure 11. Optimal profiles for S3—online optimal control.

a) Antisolvent flow-rate (FR), b) Cooling rate (CR).

Table 4. Comparison of Offline and Online Methodology in Terms of Process Kinetics and Final Batch Properties

Control methodology	Scenario	Growth accumulated (μm)	Nucleation (accumulated) (#/$g_{solvent}$)	Mean PSD (Vol%)	Yield (%)
Offline	S_1	2.3×10^{-6}	4.2	123.5	78
	S_2	8.3×10^{-7}	1.997	146.5	82
Online	S_1	7.1822×10^{-7}	1.3643	207.46	92.5
	S_2	8.5169×10^{-7}	0.7177	246.23	97.6
	S_3	8.2543×10^{-7}	1.4619	204.47	87.1

the same objective functions), and it can be accredited to the fact that the supersaturation was used more effectively during these experiments. The PSDs for experiments performed by applying optimal trajectories obtained in an offline mode, and in an online optimal control are shown in Figure 12. The improvement in the final PSD for a case of online optimal control is very obvious, and the curves show that the nucleation was minimized in each case since the curves do not show any bimodality. The general trend of results obtained by application of real-time optimal control confirmed the advantage of this methodology in comparison to the offline optimal control, which reflects the sensitivity of the former control strategy to the real time process variations. The best result in terms of the final batch properties (volume-weighted mean of 246 μm and yield of 97.6%) was obtained by applying Scenario 2 in a real-time manner, which dealt with the combination of minimization of nucleation and coefficient of variation simultaneously. The simultaneous effect of these two objectives caused the most efficient use of supersaturation, minimization of nucleation events and enhancing the growth of particles throughout the experiment.

Conclusions

A real time multivariable experimental-based optimal control methodology for the optimal quality control of an unseeded semibatch crystallization process was presented. The integration of measurements by the FBRM and ATR-FTIR into the model was established through the initial and boundary conditions of the model equations, and the optimal solution was obtained at every optimization time interval, which was set equal to 1 min. Despite the approximations used in the estimation of the nucleation and growth kinetics

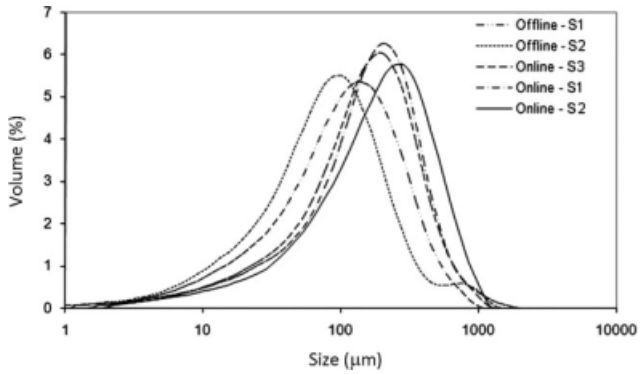

Figure 12. Particle size distribution.

and the assumption of uniform crystal shape that enabled us to use the measured CLD in the crystallizer model to perform the optimization, the results of real time multivariable optimal control showed significant improvement in the product quality. Various constrained optimization problems, which were related to the final PSD properties, such as minimization of the coefficient variation, minimization of nucleation and maximization of growth, were studied. The optimization was performed in an offline and online manner, and the results were compared in terms of process kinetics and end-of-the-batch properties.

Notation

b = nucleation constants
B = nucleation rate $\left(\frac{\text{number}}{\text{g}_{\text{solvent}}\,\text{min}}\right)$
c = optimization Constraints
ceq = equality constraint
cneq = non-equality constraint
C = concentration $\left(\frac{\text{g}_{\text{solute}}}{\text{g}_{\text{solvent}}}\right)$
CLD = Cord Length Distribution
CSD = Crystal Size Distribution
CR = cooling Rate
FR = flow rate $\left(\frac{\text{g}}{\text{min}}\right)$
g = growth constants
G = growth rate $\left(\frac{\text{m}}{\text{min}}\right)$
J = objective for optimal control
J_{goal} = goal for objective function
k_b = nucleation constant
k_g = growth constant
k_v = shape factor
L = crystal size (m)
m_w = anti-solvent mass percent
M = mass of solvent (g)
n = crystal number
N = total number of particles
P = Atr-FTIR peak
PSD = Particle Size Distribution
r = crystal size (m)
r = temperature (°C)
t = time
t_{final} = final batch time (min)

Greek letters

ΔC = supersaturation $\left(\frac{\text{g}_{\text{solute}}}{\text{g}_{\text{solvent}}}\right)$
Δt = sampling interval (min)
γ = factor that needs to be minimized
λ = objective goal
μ = moments of crystallization
ρ = solid density $\left(\frac{\text{kg}}{\text{m}^3}\right)$

Superscripts and subscripts

0 = initial
* = saturation
cont = control
g = growth
j = sampling time interval
k = control time counter
l = objective function counter
n = new particle
opt = optimization
pred = predicted
samp = sampling
w = water

Literature Cited

1. Matthews HB, Rawlings JB. Batch crystallization of a photochemical modeling, control, and filtration. *AIChE J*. 1998;44:1119–1127.
2. Armaou A, Christofides PD. Crystal temperature control in Czochralski crystal growth process. *AIChE J*. 2001;47:1:79–106.
3. El-Farra, Chiu TY, Christofides PD. Analysis and control of particulate processes with input constraints. *AIChE J*. 2001;47:8:1849–1865.
4. Ma DL, Braatz RD. Robust identification and control of batch processes. *Comput Chem Eng*. 2003;27:1175–1184.
5. Sheikhzadeh M, Trifkovic M, Rohani R. Fuzzy logic and rigid control of a seeded semi-batch, antisolvent, isothermal crystallizer. *Chem Eng Sci*. 2008;63:991–1002.
6. Gron H, Borissova A, Roberts KJ. In-process ATR-FTIR spectroscopy for closed-loop supersaturation control of a batch crystallizer producing monosodium glutamate crystals of defined size. *Ind Eng Chem Res*. 2003;42:198–206.
7. Borissova A, Dashova Z, Lai X, Roberts KJ. Examination of the semi-batch crystallization of benzophenone from saturated methanol solution via aqueous antisolvent drowning-out as monitored in-process using ATR FTIR spectroscopy. *Cryst Growth Des*. 2004; 4:1053–1060.
8. Jones AG. Optimal operation of a batch cooling crystallizer. *Chem Eng Sci*. 1974;29:1075–1087.
9. Ajinkya MB, Ray WH. On the optimal operation of crystallization processes. *Chem Eng Commun*. 1974;1:181–186.
10. Rohani S, Bourne JR. A simplified approach to the operation of a batch crystallizer. *Can J Chem Eng*. 1990;68:795–806.
11. Miller SM, Rawlings JB. Model identification and control strategies for batch cooling crystallizer. *AIChE J*. 1994;40:1312–1327.
12. Lang YD, Cervantes A, Biegler LT. Dynamic optimization of a batch cooling crystallization process. *Ind Eng Chem Res*. 1999;38: 1469–1477.
13. Mohameed HA, Abdel-Jabbar N, Takrouri K, Nasr A. Model based optimal cooling strategy for batch crystallization processes. *Chem Res Des*. 2003;81:578–584.
14. Choong KL, Smith R. Optimization of batch cooling crystallization. *Chem Eng Sci*. 2004;59:313–327.
15. Choong KL, Smith R. Novel strategies for optimization of batch, semi-batch and heating/cooling evaporative crystallization. *Chem Eng Sci*. 2004;59:329–343.
16. Costa CBB, Filho RM. Evaluation of optimisation techniques and control variable formulations for a batch cooling crystallization process. *Chem Eng Sci*. 2005;60:5312–5322.
17. Hu Q, Rohani S, Jutan A. Modeling and optimization of batch seeded cooling crystallizers. *Comput Chem Eng*. 2005;29:911–918.
18. Hu Q, Rohani S, Wang DX, Jutan A. Optimal control of a seeded batch crystallizer. *Powder Technol*. 2005;156:170–176.
19. Sarkar D, Rohani S, Jutan A. Multi-objective optimization of seeded batch crystallizaiton processes. *Chem Eng Sci*. 2006;61:5282–5295.
20. Trifkovic M, Sheikhzadeh M, Rohani S. Parameter estimation and single and multi objective optimization of a seeded, anti-solvent, isothermal batch crystallizer. *Ind Eng Chem Res*. 2008;47:1586–1595.
21. Corriou JP, Rohani S. Nonlinear control of a batch crystallizer. *Chem Eng Commun*. 2002;189:1415–1436.
22. Zhang GP, Rohani S. Online optimal control of a seeded batch cooling crystallizer. *Chem Eng Sci*. 2003;58:1887–1896.
23. Sheikhzadeh M, Trifkovic M, Rohani R. Adaptive MIMO neuro-fuzzy logic control of a seeded and an unseeded anti-solvent semi-batch crystallizer. *Chem Eng Sci*. 2008;63:1261–1272.
24. Sheikhzadeh M, Trifkovic M, Rohani R. Real-time optimal control of an anti-solvent isothermal semi-batch crystallization process. *Chem Eng Sci*. 2008;63:829–839.
25. Randolph AD, Larson MA. Theory of Particulate Processes. New York: Academic Press 1988.

Manuscript received Mar. 25, 2008, and revision received Dec. 10, 2008.